Direct Torque Control of a Synchronous Reluctance Motor Using the Finite Element Method

Sang-Don Lee †

Abstract - The construction of a Synchronous Reluctance Motor (SynRM) is simple and also highly economical because a stator from the existing AC motor can be used. Since the synchronous inductance in the Synchronous Reluctance Motor is an element that is proportional to torque, its exact value must be experimentally or analytically found for accurate control and performance development of the motor. In this paper, direct torque control (DTC) simulation is carried out to maximize the torque of the Synchronous Reluctance Motor and the fast response characteristics with the inductance value by the Finite Element Method (FEM). The response characteristics are compared through the proposed direct torque control and torque response characteristics that are based on the existing PI Control in order to confirm the fast response features. To test the performance of the direct torque controller, the torque response is analyzed with variable speed and load condition.

Keywords: direct torque control, finite element method, synchronous reluctance motor

1. Introduction

Reluctance torque is generated by the rotor of rugged construction in the Synchronous Reluctance Motor (SynRM). Its construction is simple because the rotor has neither permanent magnet nor winding, therefore high speed operation or long time operation are possible. The winding of the stator generally consists of a 3 phase sinusoid distribution, so it is very economical because a stator in the existing AC motor can be used. SynRM can decrease the torque pulsation and noise compared with the Switched Reluctance Motor, and pliant torque characteristics and science driving are possible [1-3].

Synchronous inductance is an important element in the proper construction of a synchronous motor. To improve the control and performance of the motor, locating the correct inductance value is experimentally and analytically necessary [4, 5].

A calculating equation is therefore required. We must determine the value of the inductance indirectly rather than directly when finding the value in an experiment. Doing so will raise the efficiency in applying the control with the inductance that is found through the finite element method.

The control that is based on vector control theory for the operation of the synchronous reluctance motor is used in various fields. Vector control is rather complex and requires a great deal of time for arithmetical calculation. It is quite difficult to implement a controller. On the other hand, direct torque control without the need for any complex arithmetical calculations can determine the instantaneous value of the flux and torque from the primary variable. As well, the voltage vector is controlled by the switching table, so fast torque response characteristics are obtained.

Voltage vector is determined by the region of information where the stator flux linkage is located. Research pertaining to the direct torque control that has a control structure of the simple digital form is in active progress with the switching table [6, 7].

Therefore, the finite element method was used to find the inductance of the synchronous reluctance motor and direct torque control applied as suggested in this paper. To test the fast response characteristics, we compared the response characteristics between torque response characteristics through PI control and through proposed direct torque control.

This paper also indicates torque response to test the performance of the proposed controller under the speed control of no load loss and load loss. Simulation was performed to confirm the propriety of the proposed control, and we controlled a motor with TMS320C32 DSP.

2. Modeling and Characteristic Analysis

2.1 Mathematical Modeling

The mathematical modeling of the synchronous reluc-

† Corresponding Author: Dept. of Electrical Engineering, Wonju National College, Wonju, Gangwondo, Korea. (sdlee@wonju.ac.kr)
Received October 20, 2004 ; Accepted December 29, 2004

tance motor is derivative from the variation of the rugged synchronous motor's modeling. Fig. 1 is a phasor diagram of the SynRM with equations (1) and (3) in steady state.

Equation (1) is the voltage equation of synchronous reluctance motor and is generally expressed with the rotationary reference frame as follows.

Equation (2) is the equation of motion

$$v_d = R_s i_d + L_d \frac{di_d}{dt} - \omega L_q i_q$$
$$v_q = R_s i_q + L_q \frac{di_q}{dt} + \omega L_d i_d \quad (1)$$

Where, $\omega = d\theta/dt$ [rad/sec]

$$T_e - T_l = J\frac{d\omega}{dt} \quad (2)$$

Equation (3) is shown below and it is used when expressing the magnitude of the total flux linkage with the d and q axes inductance term.

$$|\lambda| = \sqrt{(L_d i_d)^2 + (L_q i_q)^2} \quad (3)$$

Equation (4) expresses the torque equation. It can be generated in the interaction between the flux linkage and the current. The torque is proportional to inductance difference and square of the current.

$$T_e = \frac{3}{2}\frac{P}{2}(L_d - L_q) i_d i_q \quad (4)$$

Where, P indicates the number of the pole.

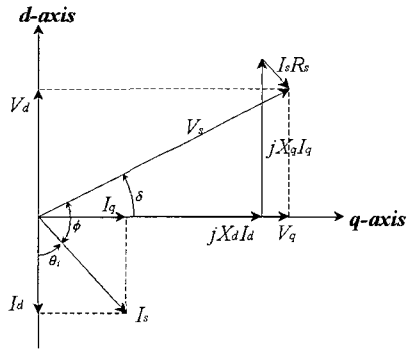

Fig. 1 Phasor diagram of the SynRM in a steady state

2.2 Characteristics Analysis

2.2.1 Model Description

Research to maximize the saliency ratio, measure the parameters such as inductance, and study design are in progress. The variables are the slot and air gap in the stator, and the rib and magnetic barrier of the rotor. To obtain the high torque and power factor characteristics while increasing the inductance difference and ratio, the variables must be determined. Table 1 presents the applied specifications of the analysis model for the synchronous reluctance motor. Fig. 2 shows the structure of the stator and the rotor, both of which are used for experimentation. For the stator, we applied the existing three phase induction motor and considered the economical efficiency.

2.2.2 d and q axes inductance calculation using FEM

The value of inductance influences the current and torque characteristics, so the method of measurement and analysis for the value was under heavy responsibility. In this paper, we have used the value of inductance that is found with the problem occurred by magnetic saturation in the analysis method and the finite element method directly [8]. In the quasi-steady state, the governing equation of finite element method from Maxwell's equation is expressed like Equation (5).

$$\frac{\partial}{\partial x}\left(\frac{1}{\mu}\frac{\partial \boldsymbol{A}}{\partial x}\right) + \frac{\partial}{\partial y}\left(\frac{1}{\mu}\frac{\partial \boldsymbol{A}}{\partial y}\right) = -\boldsymbol{J}_0 \quad (5)$$

where, $\boldsymbol{A}$ is the magnetic vector potential, μ is the permeability of the material, and $\boldsymbol{J}_o$ is the constraint current density.

To apply the finite element method in the analysis region, we have divided the entire area, S, into triangular elements, n, and found the approximate value with shape function. After all, Equation (6) is expressed as follows after applying one of the weight differential methods, or the Galerkin method where the permeability of material is isotropic.

$$\frac{1}{\mu}\int_s \sum_{j=1}^{3}\left\{\frac{\partial N_{ie}}{\partial x}\frac{\partial N_{je}}{\partial x} + \frac{\partial N_{ie}}{\partial y}\frac{\partial N_{je}}{\partial y}\right\}\boldsymbol{A}_{je}\,ds - \boldsymbol{J}_0\int_s N_{ie}\,ds = 0 \quad (6)$$

Therefore, the system matrix in the analysis region from Equation (6) is Equation (7).

$$\sum_{e=1}^{n}\left[k_{ij}^e\right]\left\{\mathrm{A}_{je}\right\} + \sum_{e=1}^{n}\left\{f_i^e\right\} = \{0\} \quad (7)$$

Where,

$$k_{ij}^e = \frac{1}{4\Delta^e}\frac{1}{\mu^e}\left(c_{ie}c_{je} + d_{ie}d_{je}\right), \quad f_i^e = \frac{-J_0\Delta^e}{3},$$

$$c_{ie} = y_{je} - y_{ke}, \quad d_{ie} = x_{ke} - x_{je},$$

Δ^e : The area of the triangular element

We used the periodical boundary condition to scrutinize 4 poles of the synchronous reluctance motor and also analyzed the half model. The number of the total elements is 18,694, and the number of the total nodes is 9,437. Fig. 3 indicates the flux distribution of the d and q axes.

Fig. 4 shows the inductance result of the *d* and *q* axes using FEM according to the currents. *q* axis inductance is constant from 2[A], which is saturated near the rib part of the rotor, but d axis inductance gradually decreases because magnetic saturation in the stator teeth, yokes, and the iron core part of the rotor is in progress.

The more the current becomes smaller under 1[A], the more d axis inductance decreases because the permeability of the iron core is almost identical in the saturation region under 0.1[T] magnetic flux density. Fig. 5 shows *d* and *q* axes inductance ratio and inductance difference. Near 1~2[A], the difference of the inductance is becoming maximum, and the inductance ratio is over 4.5 near the rated current 2.0[A].

2.2.3 Inductance measurement by AC standstill test

The inductance is measured to compare with the inductance by FEM using the stop testing method, which has slight iron loss efficiency, and the experiment is simple. Fig. 6 shows the AC standstill test. After closing b and c phases in the motor winding, the inductance from Equation (8) can be found with measuring a phase current, a phase voltage, and input. The measurement is performed with d, q axes alignment condition, and the provided frequency is 60[Hz].

$$
\begin{aligned}
&Q_a = \sqrt{(V_a I_a)^2 - P_a^2}, \qquad X_l = \omega L_l = 2\pi f L_l \\
&E = \sqrt{V_a^2 + (R_s^2 + X_l^2) I_a^2 - 2(R_s P_a + X_l Q_a)} \\
&L_{dq} = L_{dqm} + L_l = \frac{E^2}{\omega(Q_a - X_l I_a^2)} + L_l,
\end{aligned}
\tag{8}
$$

where P_a: effective power
Q_a: reactive power
X_l: leakage reactance
L_l: leakage reactance
V_a: supplied phase voltage
I_a: supplied phase current
L_{dqm}: *d*, *q* axis magnetic inductance
L_{dq}: *d*, *q* axes inductance
R_s: resistance between *b* phase and *c* phase when closing

Table 1 Specifications of the basic design model

Specification	Value	Unit	Specification	Value	Unit
Rated Power	220	W	Phase	3	
Rated Voltage	220	V	Pole	4	
Rated Current	1	A	Stack Width	50	mm
Rated Torque	0.4	Nm	Air-Gap	0.32	mm
Rated Speed	2500	Rpm	Ld	0.071	H
1's Resistance	4.2	Ω	Lq	0.016	H

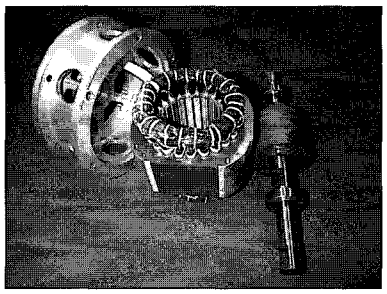

Fig. 2 SynRM photographs of stator and rotor

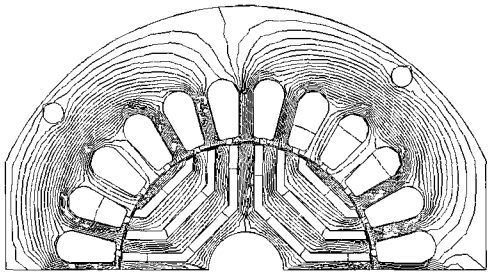

Fig. 3 Flux distribution of *d*, *q* axes

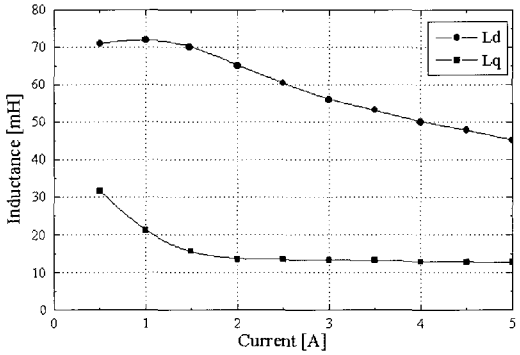

Fig. 4 *d*, *q* axes inductance of FEM

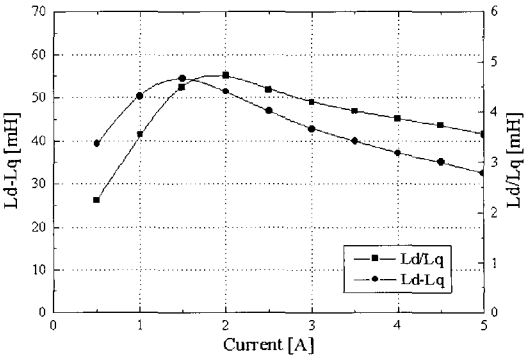

Fig. 5 L_d - L_q, L_d / L_q inductance of FEM

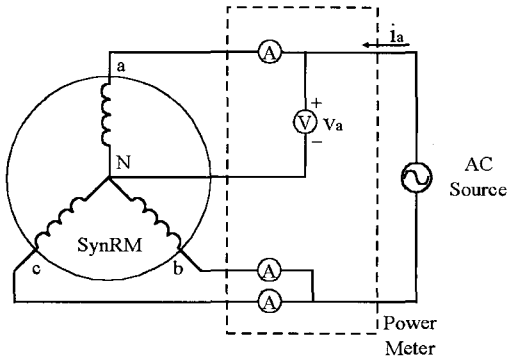

Fig. 6 Experimental configuration for AC standstill test

Fig. 7 shows the graph of the L_d and L_q through the AC testing method. Magnetic saturation does not occur with low current, so both values of the L_d and L_q are normal. That is, L_d has a small value, and L_q has a large value because magnetic saturation at the rip has not occurred yet. Fig. 8 depicts the salient pole ratio and the inductance difference. There is saturation near 1.0[A] for inductance difference, but the salient pole ratio increases to 2[A].

Table 2 indicates the comparison of inductance measurement results for FEM and for the AC standstill test. The main error in the test is normally the distortion of the supplied power and the iron loss in the AC test. Especially, the iron loss can be generated in the rotor because the rotor is fixed. Therefore, even if Equation (8) that considers the iron loss is used, *d* axis inductance still has slight error.

Table 2 Comparison of inductance measurement results

Current	Inductance	FEM	AC Test
1[A]	Ld [mH]	72.22	65.85
	Lq [mH]	20.10	17.60
2[A]	Ld [mH]	65.05	61.51
	Lq [mH]	13.60	12.92
3[A]	Ld [mH]	56.01	54.20
	Lq [mH]	12.13	11.41

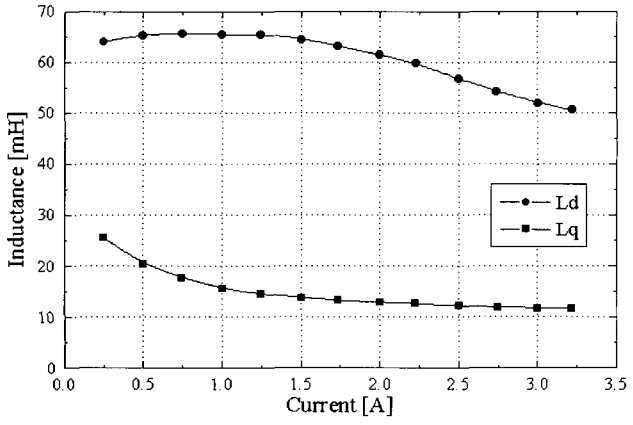

Fig. 7 *d*, *q* axes inductance of AC standstill test at 60Hz

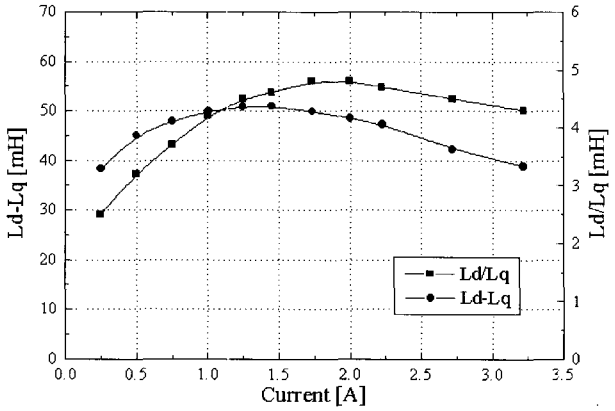

Fig. 8 L_d - L_q, L_d/L_q inductance of AC standstill test at 60Hz

3. Direct Torque Control

In direct torque control, the appropriate voltage vector makes the instant error value of the torque and linkage flux in the stator exist within the hysterisis band for each sampling time. Fig. 9 shows the principle of the direct torque control for SynRM when controlling the speed. An optimal switching voltage vector causes the real torque and real linkage flux in the stator to exist within the hysterisis band by reference torque and reference linkage flux in the stator at all times.

The voltage vector to control the magnitude of the linkage flux in the stator is divided to 6 regions as shown in Fig. 10, and 2 voltage vectors that generate the switching frequency are chosen to control the magnitude of the linkage flux in the stator.

Table 3 is for the optimal switching vector. The inputs for the switching table are the torque, the error of the linkage flux, positional information, and the voltage vector according to the switching information supplied to the converter as the output. The variable of the motor is only the resistance of the stator, so the calculation is quite simple because the linkage flux in the stator is derived from the voltage equation, and the voltage vector is always constant during each sampling time.

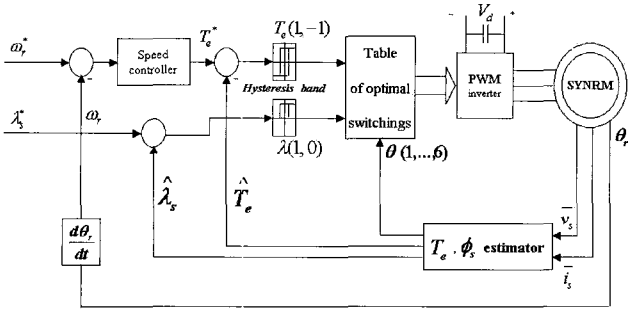

Fig. 9 DTC diagram with speed control

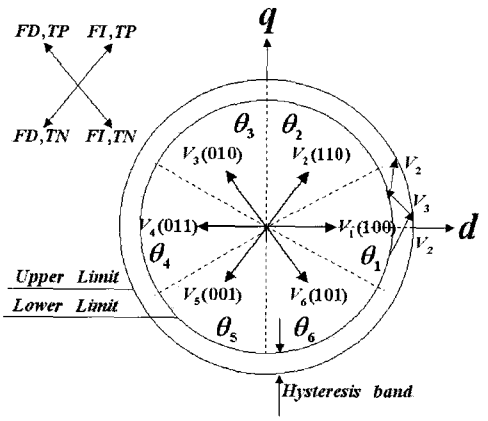

FI: flux increase; FD: flux decrease
TP: torque positive; TN: torque negative

Fig. 10 Movement of flux linkage vectors

Table 3 Optimum switching voltage vector table

Φ	T	θ					
		Θ_1	Θ_2	Θ_3	Θ_4	Θ_5	Θ_6
1	1	V_2(110)	V_3(010)	V_4(011)	V_5(001)	V_6(101)	V_1 (100)
	-1	V_6(101)	V_1(100)	V_2(110)	V_3(010)	V_4(011)	V_5 (001)
0	1	V_3(010)	V_4(011)	V_5(001)	V_6(101)	V_1(100)	V_2 (110)
	-1	V_5(001)	V_6(101)	V_1(100)	V_2(110)	V_3(010)	V_4 (011)

4. Simulation and experimental results

4.1 Simulation Result

A digital simulation was performed to confirm the propriety of the direct torque control using the proposed finite element method in this research. The manufactured synchronous reluctance motor was used for the model, and the values of all parameters are presented in Table 1.

The simulation was performed with ASCL personal software. The linkage flux has been calculated with d and q axes inductance by FEM and Fig. 9 shows the direct torque control according to the speed control. The error of the reference speed according to real torque in the direct torque control generates estimated torque by PI control, and this is the speed control at which the real generated torque in the motor follows the estimated torque.

At first, the result of the torque control and direct torque control simulation are shown in Fig. 11 to compare the torque response by PI controller. For PI control, no ripple exists because of the ideal sine wave. However, the ripple generates in a matter of fact style when driving the inverter. Although the torque ripple is more often generated in direct torque control, torque response is faster than PI control.

Fig. 12 indicates the speed and torque simulation waveform under speed control in which the no load is 0.01Nm in direct torque control. According to the rated speed, 2500rpm, the real speed control has made sufficient achievement, and the torque has also controlled with the estimated torque in a satisfactory manner.

Moreover, the real torque according to the estimated torque was calculated with the inductance that was found by the current from the proposed finite element method. Fig. 13 shows the speed and torque waveform under the rated load, 0.4Nm. It is easy to recognize that the control of the real speed and torque have made proper achievement equal to the no load. Fig. 14 presents the linkage flux waveform in the stator when controlling the speed, and the torque hysterisis bandwidth and the flux hysterisis bandwidth are 0.1 and 0.05 respectively.

4.2 Experimental Result

Fig. 15 shows the synchronous reluctance motor that was manufactured for this experiment. It consists of the main inverter circuit element that supplies power from the control input of the controller, as well as the speed and phase current detector, I/O component, and DSP component that performs algorithms such as the direct torque control and PI control. The CPU in the controller is DSP TMS320C32 in TI co. An eddy current brake is used for the load. According to the principle of the eddy current brake, there are some differences between the simulation and experiment because the brake is operated when the speed of the motor increases.

The power system obtains DC power after being put through a diode of 3-phase source voltage. It has the encoder that changes pulse output from 1024 to 4096 per 1 rotation to detect rotor position and speed on the shaft of the motor.

Fig. 16 indicates the response torque and the response of the proposed direct torque control according to the estimated torque applied under PI control. The response characteristic under direct torque control has a fast response characteristic comparing with the torque response under PI control identical to the simulation

Fig. 17 shows the response characteristic of the speed and torque when controlling no load speed in the experiment. Fig. 18 presents the response characteristic of the speed and torque when controlling load speed. The proposed direct torque control has the fast response characteristic of the torque under both no load and rated load. To measure the load, we have set a torque meter between the motor and eddy current brake that acts as one kind of load. The experiment has no reverse torque control

program.

Fig. 19 illustrates the experimental waveform of the linkage flux in the stator, and the waveform is almost identical to that of the simulation. We have set the gain of the torque hysterisis bandwidth and flux hysterisis bandwidth in the stator at 0.1.

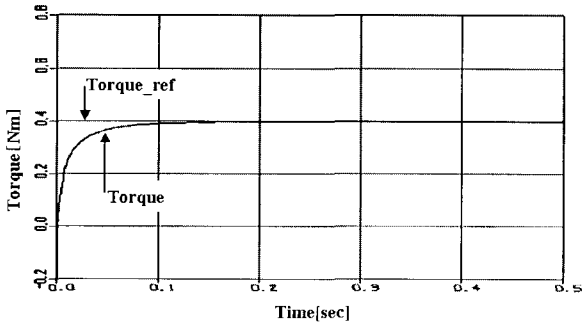

(a) Torque response of PI control

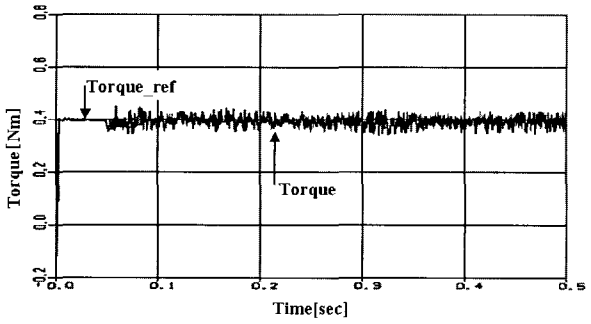

(b) Torque response of direct torque control

Fig. 11 Comparison of Torque response

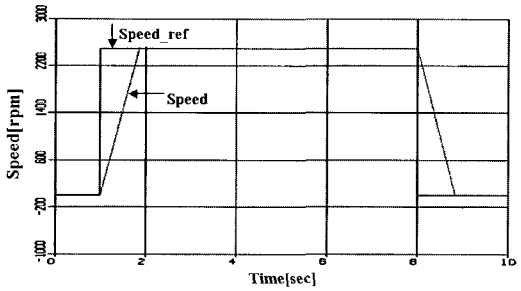

(a) Speed response of no load

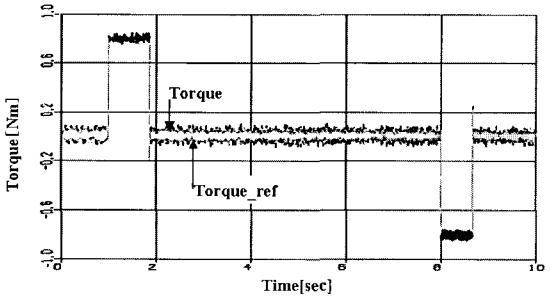

(b) Torque response of no load

Fig. 12 Speed and torque response of no load

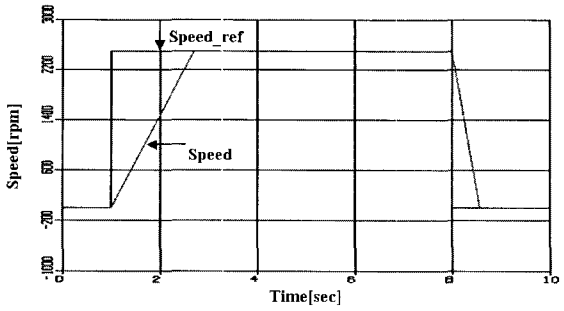

(a) Speed response of load

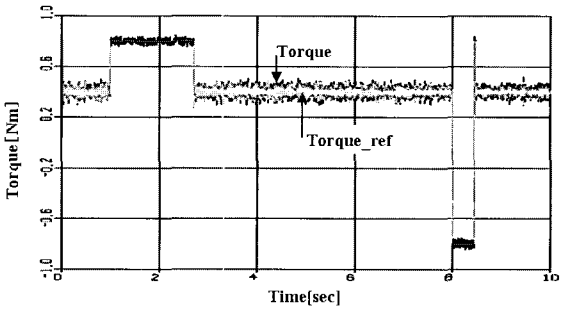

(b) Torque response of load

Fig. 13 (a) Speed and Torque response of load

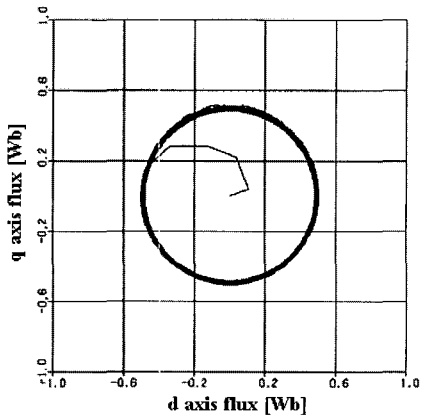

Fig. 14 Response to a flux of rated load

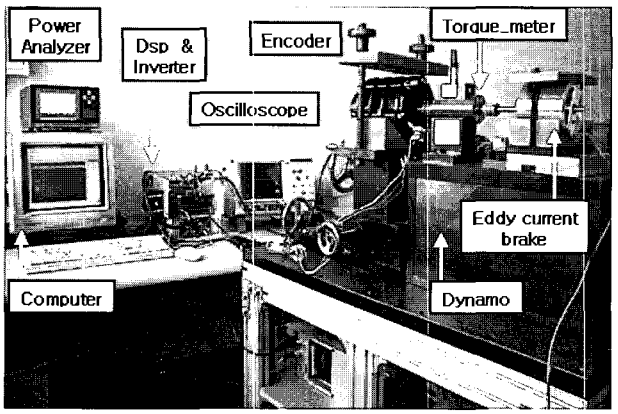

Fig. 15 Configuration of drive system under experimental conditions

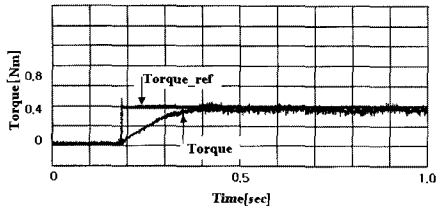

(a) Torque response of PI control

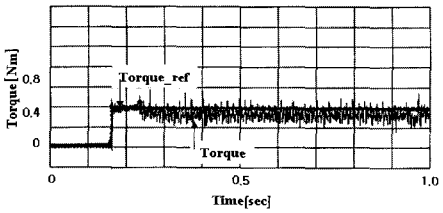

(b) Torque response of direct torque control

Fig. 16 Comparison of Torque response

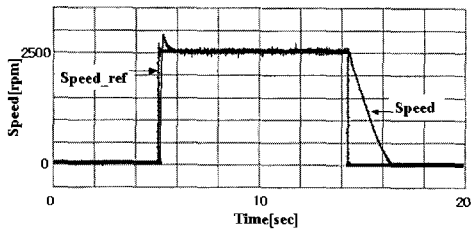

(a) Speed response of no load

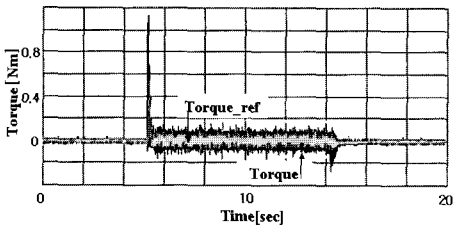

(b) Torque response of no load

Fig. 17 Speed and Torque response of no load

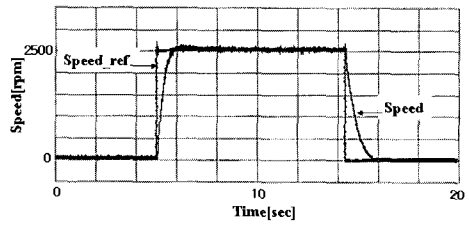

(a) Speed response of rated load

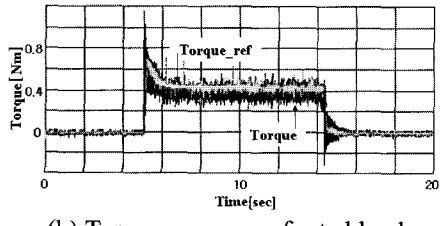

(b) Torque response of rated load

Fig. 18 Speed and torque response of rated load

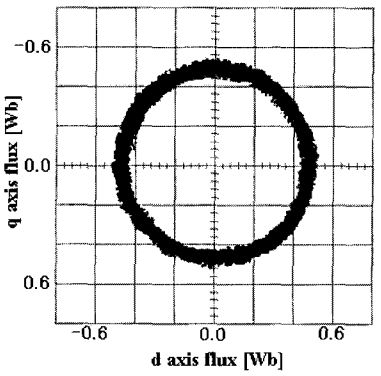

Fig. 19 Response to a flux and Current of rated load

5. Conclusion

In this paper, we have obtained the fast torque response for the high-performance operation of the variable speed driving system after proposing the direct torque control method of the synchronous reluctance motor using the inductance value by FEM. To confirm the fast response characteristic of the torque, we have compared the PI controller for the existed AC motor and the proposed PI controller in this paper. The proposed PI controller has a greater number of torque ripples but can obtain a possible high response for servos. To evaluate the performance of the proposed controller practically, the direct torque control has performed under both no-load and load experiments when controlling the speed. We have confirmed the fast response characteristics by these experiments.

References

[1] I. Boldea, "*Reluctance Synchronous Machines and Drives*," Oxford University Press Inc., New York, 1996.

[2] R.E. Betz, "Control of Synchronous Reluctance Machines" *IEEE-IAS Annual Meeting*, Detroit, pp. 456-462, Sept. 1991.

[3] T.A.Lipo, A.Vaqati ,L.Malesani, and T.Fukao, "Synchronous Reluctance motors and drives a new alternative," *IEEE-IAS Annual Meeting*, Tutorial, Oct. 1992.

[4] M. Jovanovic, "*Sensorless control of synchronous reluctance motor*," Ph.D. thesis, University of Newcastle, 1997.

[5] V.B.Honsinger, "The inductance and of reluctance machines," *IEEE Transactions on Power Apparatus and Systems*, vol PAS-90, no. 1, pp. 298-304, 1997.

[6] Peter Vas, "*Sensorless Vector and Direct Torque Control*," Oxford Press, 1998.

[7] M.R. Zolghadri, D.Diallo, D. Roye, "Direct Torque Control System for Synchronous Machine," *EPE'97*, Trondheim, pp. 3.694-3.699, 1997.
[8] Dal Ho Lim, "Finite Element Method of Magnetic Field" Dong Myung Publishing Co., 1992.

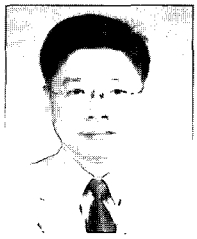

Sang-Don Lee
Birthday: July 14, 1958
1996 Ph.D Electrical Engineering, Hanyang University
1986 M. Eng., Electrial Engineering, Hanyang University
1981 B.S., Elecrical Engineering, Hanyang University
1995 ~ Present Associate Professor of Wonju National College
1988 ~ 1995 Senior Researcher of Agency for Defense Development